**ISSN: 2037-7738**
GRASPA Working Papers
[online]

# Web Working Papers
by
The Italian Group of Environmental Statistics

Gruppo di Ricerca per le Applicazioni della Statistica
ai Problemi Ambientali

www.graspa.org

## Multiresolution analysis of spatial patterns to detect dominant directions

Jorge Mateu, Orietta Nicolis

GRASPA Working paper n.44, February 2012

# Multiresolution analysis of spatial patterns to detect dominant directions

**Jorge Mateu**

Department of Mathematics, Universitat Jaume I, E-12071 Castellon, Spain

*email:* mateu@mat.uji.es

**and**

**Orietta Nicolis**

Department of IT and Mathematical Methods, University of Bergamo, I-24044 Dalmine, Italy

*email:* orietta.nicolis@unibg.it

Summary: The assumption of direction invariance, i.e., isotropy, is often made in the practical analysis of spatial point processes due to simpler interpretation and ease of analysis. However, this assumption is many times hard to find in real applications. Many homogeneous point processes are indeed anisotropic. This paper concerns the analysis and detection of spatial anisotropies in terms of detection of linearities in spatial point processes, and even more generally, in terms of testing for spatial anisotropy.

We propose a wavelet-based approach to test for isotropy in spatial point processes based on the logarithm of the directional scalogram. Under the null hypothesis of isotropy, a random isotropic process should be expected to have the same value of the directional scalogram for any possible direction. Hence, Monte Carlo simulations of the logarithm of the directional scalograms over all directions are used to approximate the test distribution and the critical values. We demonstrate the efficacy of the approach through simulation studies and an application to a desert plant data set, where our approach confirms suspected directional effects in the spatial distribution of the desert plant species.

Key words: *Ambrosia dumosa*, Anisotropy, Directional wavelets, Scalogram, Spatial point patterns.

[1]Corresponding author: Jorge Mateu. *Email address*: mateu@mat.uji.es. *Fax*: +34.964.728429

## 1. Introduction

Spatial point process models are useful tools to model irregularly scattered point patterns that are frequently encountered in biological, ecological, and epidemiological studies; examples include locations of biological cells in a tissue, trees in a forest, or leukemia patients in a state. A spatial point pattern is a set of points $\{\mathbf{x}_i \in A : i = 1, \ldots, n\}$ for some planar region $A$. Very often, $A$ is a sampling window within a much larger region and it is reasonable to regard the point pattern as a partial realization of a stochastic planar point process, the events consisting of all points of the process which lie within $A$. Let $N$ be this stochastic planar point process defined on $\mathbb{R}^2$ but observed on a finite observation window $W$. For an arbitrary set $A \in \mathbb{R}$, let $|A|$ and $N(A)$ denote the area of $A$ and the number of events from $N$ that are in $A$, respectively.

The mathematical theory of point processes was first developed in order to solve various problems where it is sensible to model the locations of events as random. Indeed, the study of spatial point patterns has a long history in ecology and forestry (Goodall, 1952; Pielou, 1977; Ripley, 1981). Spatial point patterns have also found application in fields as diverse as archeology (Hodder and Orton, 1976), cosmology (Neyman and Scott, 1958), geography (Cliff and Ord, 1981), seismology (Ogata, 1998) and epidemiology (Diggle and Richardson, 1993). Recent textbooks related to the topic of analysis and modeling of point processes include Stoyan *et al.* (1995), Diggle (2003), Baddeley *et al.* (2006), Illian *et al.* (2008), or Gelfand *et al.* (2010). The concept of *complete spatial randomness* (CSR) is fundamental to the quantitative description of a spatial pattern. A formal definition of CSR is that the events in the region of observation $A$ constitute a partial realization of a homogeneous, planar Poisson process (Diggle, 2003). This process incorporates a single parameter, $\lambda$, the intensity, or mean number of events per unit area. The actual number of events in $A$, $n$ say, is an observation from a Poisson distribution with mean $\lambda\,|A|$, where $|A|$ denotes the area of the region $A$.

A point process is stationary and isotropic if its statistical properties do not change under translation and rotation, respectively. Informally, *stationarity* implies that you can estimate properties of the process from a single realization on $A$, by exploiting the fact that these properties are the same in different, but geometrically similar, subregions of $A$; *isotropy* means that there are no directional effects.

Let $d\mathbf{x}$ denote a small region containing the point $\mathbf{x}$. The *first-order intensity function* of a spatial point process is defined as $\lambda(\mathbf{x}) = \lim \{\mathbb{E}[N(d\mathbf{x})]/|d\mathbf{x}|\}$ when $|d\mathbf{x}| \to 0$. Intuitively, $\lambda(\mathbf{x})|d\mathbf{x}|$ is the approximate probability for $d\mathbf{x}$ to contain exactly one event from $N$. If we assume stationarity and isotropy, then $\lambda(\mathbf{x}) \equiv \lambda = \mathbb{E}[N(A)]/|A|$, (constant, for all $A$). Thus, if the process is homogeneous the intensity function reduces to a constant, $\lambda$, equal to the expected number of events per unit area.

The assumption of isotropy is often made in practice due to simpler interpretation and ease of analysis. However, stationarity and/or isotropy are many times hard to find in real applications. Many homogeneous point processes are indeed anisotropic. There are many varied forms of anisotropy: (a) anisotropic arrangements of the points; (b) anisotropic behavior of marks if they describe orientations; (c) combination of anisotropic point distribution and anisotropic mark behavior. Orientation analysis is the quantification of the degree of anisotropy in the case of non-isotropic point patterns and the detection of inner orientations in case of isotropy (Ohser and Stoyan, 1981; Stoyan and Benes, 1991; Mateu, 2000; Redenbach *et al.*, 2009). Typical examples of oriented point patterns are patterns in which the points lie randomly in parallel strips of random or constant breadth (anisotropic case) or on an isotropic system of random fibres (inner orientation). Anisotropy is the converse of isotropy but it has many different aspects. A given pattern may appear as isotropic with respect to one aspect, whilst it is in fact anisotropic when considering another aspect. For example, if a structure consists of isolated particles, then the arrangement of the particles may be anisotropic, whilst the particles are isotropic. It is also possible that the arrangement is isotropic whilst the particles are anisotropic. For example, the anisotropy (directionality) is a significant property of images. The anisotropy may be the result of the process by which the imaged object might have been formed. Thus, on numerous occasions anisotropy reflects properties and determines the behavior of the textured objects. The importance of anisotropy in visual perception and object characterization inspired a range of studies for anisotropy analysis (Kovalev and Bondar, 1997). Anisotropy can be present when the spatial point patterns contain points placed roughly on line segments. See details in Møller and Rasmussen (2009) who consider a particular class of point processes whose realizations contain such linear structures. Blackwell (2001), Blackwell and Møller (2002) consider point process models with linear structures close to the edges of (deformed) Dirichlet (or Voronoi) tessellations. However, the exact mechanism responsible for the formations of lines is unknown. Thus the development of tractable and practically useful spatial point process models capable of producing point patterns with linear structures becomes important (Penttinen and Stoyan, 1989).

The arguments shown and the literature involved in the analysis and detection of spatial anisotropies sets a motivating research line in terms of detection of linearities in spatial point patterns, and even more generally, in terms of testing for spatial anisotropy. Here we understand spatial anisotropy as the presence of main directions in the point pattern (Schenk and Mahall, 2002).

Ohser and Stoyan (1981) and Rosenberg (2004) have proposed methods to assess isotropy (and to consequently detect anisotropy) for spatial point processes. These approaches, however, are limited to certain classes of models. Guan *et al.* (2004, 2006) propose a formal nonparametric approach to test for isotropy based on the asymptotic joint normality of the sample second-order intensity function. They derive a $L_2$ consistent subsampling estimator for the asymptotic covariance matrix of the sample second-order intensity function and use this to construct a test statistic with a $\chi^2$ limiting distribution. The authors state that their approach requires only mild moment conditions and a weak dependence assumption for the underlying process. However, we argue that their approach is based on asymptotic results (not often attainable in practical situations) and can be considered quite technical for the vast majority of practitioners. Alternative methods based on two-dimensional spectral analysis were proposed by Mugglestone and Renshaw (1998) to calculate objective estimates of the orientation and frequency of geological lineations from digitised images obtained from aerial photographs of glaciated terrain in northern Canada. However, the complications inherent in spectral analysis (particularly for more than one dimension) appear to have discouraged applied statisticians and ecologists from making use of these methods.

Wavelet analysis has succeeded in a variety of applications and held promise in the area of spatial pattern analysis (e.g. Donoho, 1993; Gao and Li, 1993; Grenfell *et al.*, 2001). As a flexible tool, wavelet analysis provides many advantages over other methods of analyzing data series from one-dimensional transect. The main advantages are its ability to preserve and to display locational information, while the approach allows for pattern decomposition, and it does not require stationarity of the data. Despite its advantages, wavelet analysis has only been involved in several works for detection of patterns (e.g. Saunders *et al.*, 1998; Brosofske *et al.*, 1999; Harper and Macdonald, 2001; Perry *et al.*, 2002).

Our goal in this paper is to detect anisotropy in terms of pinpointing main directions using directional wavelets applied over a raw estimation of the spatial intensity through a quadrat counting method. We show the efficacy of this approach through simulated examples, and we further propose a statistical test to assess for isotropy. An application to a field data set of a complete 1984 census of 4358 *Ambrosia dumosa* plants is also considered. The rest of the article is organized as follows. Section 2 provides the basics of directional wavelets as a tool to detect main directions, and show their performance through several simulated examples. Section 3 develops a statistical test and analyzes its (type I error and power) properties. We apply this testing approach to the *Ambrosia dumosa* data set in Section 4. The paper ends with some points for further discussion.

## 2. A wavelet approach

Wavelets are mathematical functions with zero mean and moderate decay such that they are non-zero only over a small region. They can be defined as translations and re-scales of a single squared-integrable function $\psi(x) \in \mathbb{L}_2(\mathbb{R})$, called *the wavelet function* or *the mother wavelet*, as

$$\psi_{a,b}(x) = \frac{1}{\sqrt{|a|}}\psi\left(\frac{x-b}{a}\right). \tag{1}$$

where $a \in \mathbb{R}\backslash\{0\}$ and $b \in \mathbb{R}$ are the scale and shift parameters, respectively. Normalization by $\frac{1}{\sqrt{|a|}}$ ensures that the energy of the corresponding wavelet is independent of $a$ and $b$, i.e.

$$\int_{-\infty}^{\infty} |\psi_{a,b}(x)|^2 = \int_{-\infty}^{\infty} |\psi(x)|^2.$$

For any function $f(x) \in \mathbb{L}_2(\mathbb{R})$, the continuous wavelet transform is given by

$$W_f(a,b) = \langle f, \psi_{a,b}\rangle = \int_{\mathbb{R}} f(x)\overline{\psi_{a,b}(x)}dx, \tag{2}$$

where the overline denotes complex conjugate. The two dimensional extension of (2) is straightforward. By denoting with $\mathbf{x} = (x, y)$ and $\mathbf{b} = (b_1, b_2)$ a spatial location and the translations, respectively, (2) for $f(\mathbf{x}) \in \mathbb{L}_2(\mathbb{R}^2)$ can be written as

$$W_f(a,\mathbf{b}) = \langle f, \psi_{a,\mathbf{b}}\rangle = \int_{\mathbb{R}^2} f(\mathbf{x})\overline{\psi_{a,\mathbf{b}}(\mathbf{x})}d\mathbf{x}, \tag{3}$$

Several wavelets has been proposed in literature. Although the first wavelet was introduced by Haar (1910), the study of wavelets reaches its maximum development after the work of

Goupillaud *et al.* (1984). Since this period we can find an explosion of scientific activity in a wide variety of fields (see, for example, Mallat (1999) or Vidakovic (1999)).

### 2.1 *Directional wavelets*

For $\mathbf{x} \in \mathbb{R}^2$, and any function $f(\mathbf{x}) \in \mathbb{L}_2(\mathbb{R}^2)$, the continuous directional wavelet transform for a scale $a$ and an orientation $\theta$ is given by

$$W_f(a, \mathbf{b}, \theta) = \langle f, \psi_{a,\mathbf{b},\theta} \rangle = \int_{\mathbb{R}^2} f(\mathbf{x}) \overline{\psi_{a,\mathbf{b}}(\mathbf{x}, \theta)} d\mathbf{x}. \tag{4}$$

In literature, a variety of directional wavelets $\psi_{a,\mathbf{b}}(\mathbf{x}, \theta)$ have been proposed. In particular Neupauer and Powell (2005) introduced a flexible function called fully-anisotropic directional Morlet wavelet, and is given by

$$\psi_{a,\mathbf{b}}(\mathbf{x}, \theta) = e^{i\mathbf{k_0} \cdot \mathbf{Cx}} e^{1/2 \mathbf{Cx} \cdot \mathbf{A}^T \mathbf{ACx}} \tag{5}$$

where $\mathbf{k_0} = (0, k_0)$ is a wave vector with $k_0 \geqslant 5.5$, $\mathbf{A} = diag(D, 1)$ denotes a diagonal matrix, and $D$ is the anisotropy ratio defined as the ratio of the length of the elliptical envelope in the $y$-direction to the length of the elliptical envelope in the $x$-direction. The matrix $\mathbf{C}$ is a linear transformation given by

$$\mathbf{C} = \begin{pmatrix} cos\theta & sin\theta \\ -sin\theta & cos\theta \end{pmatrix}$$

This transformation rotates the entire wavelet through an angle $\theta$ defined as positive in the counterclockwise direction. Two examples of this fully-anisotropic wavelet for directions $\theta = 30, 90$ are shown in Figure 1.

[Figure 1 about here.]

In order to identify the behavior of the process in different directions, Kumar (1995) introduced two new functions, $\eta(a, \theta)$ and $\zeta(a, \theta)$, given by

$$\eta(a, \theta) = \int |W_f(a, \mathbf{b}, \theta)|^2 d\mathbf{b} \tag{6}$$

and

$$\zeta(a,\theta) = \frac{\eta(a,\theta)}{\int \eta(a,\theta)d\theta}. \tag{7}$$

The component $|W_f(a, \mathbf{b}, \theta)|^2$ in (6), called *directional scalogram*, gives the distribution of the energy of a function at location $\mathbf{x}$, scale $a$ and direction $\theta$. Hence, $\eta(a, \theta)$ characterizes the distribution of the energy at different scales and directions, whereas $\zeta(a, \theta)$ provides the relative distribution of the energy in different directions at a particular scale.

In practice, (6) and (7) can be implemented by discretizing the parameters $\theta$, $a$ and $\mathbf{b}$ into a fine grid covering the corresponding parameter space. Thus we can define a set of $\theta_i \in (0, \pi]$ with $i = 1, \ldots, m$ directions, $a_j$ with $j = 1, ..., L$ scales, and finally $\mathbf{b}_k$ with $k = 1, ..., N$ spatial coordinates. The computation of $\eta(a_j, \theta_i)$ can be done by numerically integrating the resulting scalogram over the domain of $\mathbf{b}$.

## 2.2 *Wavelet analysis of spatial point processes*

The method proposed by Neupauer and Powell (2005) can be used for detecting anisotropy in images, that is pixels located on a regular grid. Only few works consider the wavelet transforms of spatial point processes. Most of them assumes isotropic processes and use the Haar wavelet for the estimation of intensity function (De Miranda, 2008). However, the statistical properties of these wavelet estimators are not easily derived.

Since our aim is testing for anisotropy through identification of dominant directions in spatial point patterns, we suggest considering the fully-anisotropic Morlet wavelet proposed by Neupauer and Powell (2005). This directional wavelet is applied over a quadrat counting-based estimation of the first-order intensity of the point pattern. In quadrat counting, the window $A$ is divided into subregions $A_1, ..., A_m$ (quadrats) of equal area. We then count the numbers of points falling in each quadrat, $n_j = N(\mathbf{x} \cap A_j)$ for $j = 1, \ldots, m$. These are unbiased estimators of the corresponding intensity measure values (Illian *et al.*, 2008). Quadrat counting has also a nice advantage, and it is that if we choose the quadrats in a meaningful way, for example defining the quadrats using covariate information, we take advantage of the spatial covariance-based information. By application of the continuous fully-anisotropic Morlet wavelet transform over the resulting quadrat counts we obtain $W_{\hat{\lambda}}(a, \mathbf{b}, \theta)$, and the corresponding $\eta(a, \theta)$ values for each scale and direction are evaluated. This approach allows to: (a) identify anisotropic linear patterns, (b) estimate dominant directions, (c) build a statistical test for isotropy.

In particular, dominant directions are identified by the largest values of $\eta(\cdot, \cdot)$ and $\zeta(\cdot, \cdot)$ in the scalogram plot. In addition, several features of linear patterns, such as localization and standard deviation, can be highlighted by plotting the wavelet coefficients relative to the largest values of the directional scalogram. As an example, the first two rows in Figure 2 show a simulated example of a spatial pattern with a marked main direction at 45 degrees. The corresponding values of $\eta(a, \theta)$ for a set of scales, angles, and several levels of resolutions are shown; the main direction is clearly detected. In contrast, the last row in Figure 2 shows a random isotropic point pattern and the corresponding values of $\eta(a, \theta)$. As expected no main direction is detected.

[Figure 2 about here.]

## 2.3 *Simulated examples*

We considered different scenarios of spatial point patterns with an average size of 1000 points on the unit square. We simulated realizations from a Poisson process and added a set of points defining particular directions. For illustration purposes, three examples of added sets of points were used: (a) one linear pattern, (b) two linear patterns, and (c) parallel linear patterns.

Each linear pattern was simulated using a linear regression model $y_i = \beta_0 + \beta_1 x_i + \epsilon_i$, with $\epsilon_i \sim N(0, \sigma)$ and $i = 1, \ldots, n_p$ where $n_p$ is the number of simulated points $(x_i, y_i)$, and $\sigma$ the standard deviation of $\epsilon_i$. Parameter $\beta_1$ represents the direction $\theta$ of the linear (anisotropic) component. For each pattern with a given number of points over the unit square, we considered several values for $(\beta_0, \beta_1, \sigma)$. Each scenario was repeated 100 times, and for each particular point pattern the fully-anisotropic Morlet wavelet with $k_0 = 5.5$ and $D = 0.1$ (see right plot in Figure 1) was applied over a quadrat counting-based estimation of the first-order intensity of the point pattern. These Morlet wavelet parameters were chosen in terms of a better adaptation to the detection of linearities in point patterns.

2.3.1 *One linear pattern.* We simulated point patterns formed by 70% of purely random points generated by an isotropic Poisson process in the unit square, and 30% of points belonging to a directional pattern representing the anisotropic component. In particular, the linear pattern is the output of a regression model with slope $\theta$ and zero mean Gaussian errors with a standard deviation of $\sigma = 0.1$. Figure 2 shows an example of a simulated point pattern with $N = 1000$ points in the unit square with a marked directional pattern of 45 degrees. The $\eta(\cdot,\cdot)$ values show that the largest fraction of energy of the wavelet coefficients is concentrated around the preferential direction of 45 degrees. This becomes clearer if we observe the $\eta(\cdot,\cdot)$ behavior for some selected levels of resolution (see Figure 2c). Since the maximum peaks are reached for scales 25 and 30, these levels of resolution contain the most important information on the anisotropic component of the data. The representation of the wavelet coefficients in Figure 2d for $L = 25$ allows to localize the dispersion of the points around the identified linear structure.

To show that the wavelet approach is not sensible to a particular direction, we repeated the experiment for different types of linear patterns. Results from anisotropic simulated spatial point patterns with dominant directions of $\theta = 30, 60$ and 135 are shown in Figure 3.

[Figure 3 about here.]

We note that in each case the directional scalogram highlights the largest values of $\eta(\cdot,\cdot)$ around the same level of resolution ($L = 20$). This is because the scale parameter in the wavelet transform represents the variability of the main pattern. If we compare these results with those obtained in the case of a purely random pattern in Figure 2e, we note many differences. In the isotropic point pattern the largest fraction of energy is concentrated in the finest levels of resolution, and the $\eta(\cdot,\cdot)$ values are approximatively the same for each level of resolution without showing any significant dominant direction (see Figure 2f).

To show the ability of the wavelet method in estimating the dominant direction, we simulated 100 data sets for each type of linear pattern ($\theta = 30, 60$, and 135) and we then estimated the dominant directions. The results are shown in Table 1. In all cases the estimated directions resulted very close to the parameters used to simulate the linear pattern. The low values of standard deviations for the anisotropic cases compared with those values under the isotropic pattern indicate the robustness of the method in both assessing anisotropy and estimating the main direction present in the data.

[Table 1 about here.]

2.3.2 *Two linear patterns.* We considered two cases of spatial point patterns with two dominant directions. We first simulated a spatial point pattern with $N = 1000$ points in the unit square with two perpendicular linear patterns with slopes $\theta_1 = 45$ and $\theta_2 = 135$ (Figure 4). The standard deviation of the errors of the regression defining the linear patterns was fixed to $\sigma = 0.1$. The directional scalogram reaches its maximum at 45 and 135 degrees, at the scales between 20 and 25. The wavelet coefficients at ($\theta_1 = 45$; $L = 20$) and ($\theta_2 = 135$; $L = 25$) correctly detect the position and the variability of the anisotropy.

[Figure 4 about here.]

A second case, not shown here to save space, regards a simulated data set with two marked linear patterns having different slopes and variability. One strip is characterized by a slope of $\theta_1 = 60$ degrees and an error distribution given by $N(0, \sigma_1 = 0.04)$; the second strip has a slope of $\theta_2 = 135$ degrees with an error distribution given by $N(0, \sigma_2 = 0.08)$. The directional scalogram clearly detects these two directions (60 and 135 degrees) with maximum values at levels of resolution $L = 10$ (for the linear pattern of 60 degrees) and $L = 20$ (for the linear pattern of 135 degrees). This means that the scale is strictly correlated with the variability of the data. The wavelet coefficients at ($\theta_1 = 60$; $L = 10$) and ($\theta_2 = 135$; $L = 20$) correctly detect the position and the variability of the anisotropy.

To analyze the ability of the wavelet method in estimating the two dominant directions, we simulated 100 data sets for each type of point processes considered in this Section. A summary of the results is shown in Table 2 (columns related to TLP1 and TLP2). In all cases the estimated directions resulted very close to the parameters used to simulate the linear pattern. Again the lowest standard deviation corresponded to the scale with maximum peak in the directional scalogram. For example, the angle estimation for those data sets simulated with a marked directionality at $\theta_1 = 60$ and $\theta_2 = 135$ showed lowest standard deviations at scales $L = 10$ and $L = 20$, respectively. This reflects the different variability of errors for the two linear patterns.

[Table 2 about here.]

2.3.3 *Parallel patterns.* We finally considered simulated point patterns with five parallel linear patterns, each one with a slope of 45 degrees, as shown in Figure 5a. The simulated patterns are formed by $N = 1000$ points in the unit square: 60% was generated by parallel linear patterns with Gaussian errors, $N(0, 0.06)$ (20% per each pattern), and the rest 40% was generated following an isotropic random pattern.

The directional scalogram in Figure 5b shows that the wavelet method is able to detect the parallel patterns. The levels of resolution $L = 15 - L = 30$ identify the main directions of anisotropy (equal to 45 degrees). We note an interesting comparison between the directional scalogram for the case of parallel patterns (Figure 5b) and the case where there is only one pattern (Figure 2b): while in Figure 2b the scalogram has a bulb shape due to larger variability of the coefficients at lower levels of resolution, the scalogram in Figure 5b shows an elongated shape showing that the main direction of 45 degrees can be detected at different scales.

The highest peak of Figure 5c highlights the scale $L = 15$ as the level of resolution with the maximum energy. Hence, the wavelet coefficients at this scale identify the number of patterns in the data, their spatial location and their variability (Figure 5d). One hundred repetitions of simulated point patterns with $N = 1000$ points in the unit square showing five parallel strips with a marked directionality of 45 degrees reported the results shown in Table 2 (PP).

[Figure 5 about here.]

## 3. A test for isotropy

### 3.1 *Method*

Let $\hat{\lambda}(\mathbf{x})$ be the estimated first-order intensity function by the quadrat counting method, where $\mathbf{x}$ denotes the spatial locations. This is an unbiased estimator of the corresponding intensity measure values (Illian *et al.*, 2008). Assume we have $m$ possible directions $\theta_i \in (0, \pi]$ with $i = 1, \ldots, m$, $L$ possible scales $a_j$ with $j = 1, \ldots, L$, and $N$ points, $\mathbf{b}_k$, with $k = 1, \ldots, N$. By applying the directional wavelet we obtain the directional scalogram $W_{\hat{\lambda}}(a_j, \mathbf{b}_k, \theta_i)$ giving the distribution of the energy of $\hat{\lambda}(\mathbf{x})$. This scalogram is obtained for a range of scales and orientations at all positions in the domain of $\hat{\lambda}(\mathbf{x}_i)$. Denote by $\overline{S}_{\theta_i, a_j}$ the variance of the corresponding wavelet coefficients for a particular direction $\theta_i$ and a scale $a_j$. $\overline{S}_{\theta_i, a_j}$ can be considered the practical implementation of the $\eta(a, \theta)$ function in (6), and thus is given by

$$\overline{S}_{\theta_i, a_j} = \frac{1}{N} \sum |W_{\hat{\lambda}}(a_j, \mathbf{b}_k, \theta_i))|^2. \tag{8}$$

Under isotropy, we should expect having the same value of the directional scalogram for all possible directions, and thus we should expect $\overline{S}_{\theta_i,a_j} = \overline{S}_{\theta_j,a_j}$ for any two directions. Since the mean of the logarithm of the variance of the wavelet coefficients is approximately Normal distributed under isotropy, we consider the following test statistic

$$T(\theta_i) = \frac{1}{L}\sum_j \log \overline{S}_{\theta_i,a_j}, \tag{9}$$

as a statistical test of isotropy for point processes. Under the null hypothesis of isotropy, this statistical test should take similar values for each direction $\theta_i$, that is $T(\theta_1) = \ldots = T(\theta_i) = \ldots = T(\theta_{180})$, whereas under the alternative hypothesis, there should be al least one direction $\theta_0$ with corresponding values of $T(\theta_0)$ statistically different from the values of the statistical test evaluated in other directions.

### 3.2 *Statistical properties*

The statistical properties, type I error rate and power of the test, were analyzed by simulations. We considered different scenarios representing several possibilities. We simulated spatial point patterns on the unit square with the following characteristics: (a) Varying number of points, $N = 1000$ and $N = 300$; (b) One marked main direction at 45 degrees, and two main directions at 30 and 120 degrees; (c) Varying variability within the linear structures: $\sigma = 0.06, 0.10, 0.40$.

For the evaluation of the type I error rate, we simulated 1000 isotropic patterns for each size ($N = 1000$ and $N = 300$). The power of the test was analyzed running the test over 1000 anisotropic patterns generated according to the previous considered scenarios. Given a simulated point pattern we obtained 180 values of the test statistic $T(\theta_i)$ for each $\theta_i = 1, \ldots, 180$. And this was repeated 1000 times.

For each $\theta_i$, the first 500 values were used to determine the empirical distribution of $T(\theta_i)$, and this is shown in form of histogram in Figure 6. The other 500 values were used to accept or reject the null hypothesis by comparing with the empirical distribution of $T(\theta_i)$. By looking at Figure 6 we note a clear difference between the empirical distribution of $T(\theta_i)$

under isotropic and anisotropic scenarios. Note that this difference is higher for those point patterns with smaller standard deviations within the linear structures.

[Figure 6 about here.]

Type I error rates and powers of the test are given in Figure 7. For each direction $\theta_i$, the type I error rate $\alpha_{\theta_i}$ is evaluated by the number of rejected over 500 cases under the null hypothesis of isotropy, and the power $1-\beta$ is given by the number of rejected over 500 cases under the alternative hypothesis of anisotropy. Hence, for each one of the considered scenarios we have 180 values of $\alpha$ and $1-\beta$.

In particular, first row in Figure 7 shows the values of $\alpha$ and $1-\beta$ for each direction $\theta_i$ for $i = 1, \ldots, 180$ when we have $N = 1000$ points in the unit square, and the anisotropic spatial pattern is given by a linear structure at direction 45 degrees. Three different standard deviations for the linear model were considered under the alternative hypothesis ($\sigma = 0.06, 0.10, 0.40$). Note that most of the $\alpha$ values are lower than the threshold value of 0.05, and the power is often larger than 0.95. As expected, the highest values of the power were concentrated around the true direction of 45 degrees. The lowest values of the power refer to those cases where the variability was highest (for example, $\sigma = 0.40$). Similar considerations can be followed for the other cases in rows two to four in Figures 7. Our results suggest that the proposed statistical test can be used as a reasonable measure of the degree of anisotropy, and thus can be used in practice for the statistical analysis of anisotropic spatial point patterns.

[Figure 7 about here.]

## 4. Application to Ambrosia dumosa Data

In this section, we apply the proposed testing method to the *Ambrosia dumosa* data (Miriti *et al.*, 1998). The data consist of locations of 4358 *Ambrosia dumosa* plants, recorded in the

1984 census within a square hectare ($100 \times 100\ m^2$) area in the Colorado Desert (Figure 8). *Ambrosia dumosa* is an extremely abundant, long-lived, and drought deciduous shrub which is often found on well-drained soils below 1061-m elevation (Miriti *et al.*, 1998). In the study site, it accounts for approximately 62% of all the encountered perennial plant species.

Previous studies of the *Ambrosia dumosa* data have focused on detecting clustering and assessing the effects of possible intra-specific interaction on the mortality of juvenile plants under the assumption of isotropy (Miriti *et al.*, 1998). Several authors (Perry *et al.*, 2002; Rosenberg, 2004 or Schenk and Mahall, 2002) noted graphical evidence of anisotropic patterns of the *Ambrosia dumosa* locations arguing that the effects of directional shading on germinating seeds and young seedlings may cause anisotropy of *Ambrosia dumosa* locations (between seedlings and adult plants) in the north-south, northwest-southeast, and eastwest directions.

Figure 8 (first row) shows the wavelet analysis of the *Ambrosia dumosa* data set: the directional scalogram identifies a main dominant direction around 165 degrees and a second (perhaps less important) direction around 43 degrees.

[Figure 8 about here.]

We conducted a comparative analysis evaluating the test statistic $T(\theta_i)$ for $i = 1, \ldots, 180$ under 1000 simulated isotropic point patterns with the same number of points as the *Ambrosia dumosa* in the unit square, and under the *Ambrosia dumosa* data set itself. The summary statistics for $T(\theta_i)$, $i = 1, \ldots, 180$ revealed that the values of $T(\theta_i)$ are clearly larger for the *Ambrosia dumosa* data set, suggesting the presence of an anisotropic pattern.

We then applied our statistical test over the *Ambrosia dumosa* (see second row in Figure 8). The histogram of $T(\theta_i)$, $i = 1, \ldots, 180$ under 1000 isotropic simulations shows, as expected, a normal distribution, and it is used to build confidence intervals for the mean of the test statistic under isotropic patterns. Indeed, Figure 8e confirms that the values of $T(\theta_i)$,

$i = 1, \ldots, 180$ for the *Ambrosia dumosa* data set stay away from the confidence interval under the null hypothesis of isotropy. Finally, the $p$-values for the *Ambrosia dumosa* data set confirm a strong evidence against the assumption of isotropy, which agrees with the findings/hypotheses in previous studies.

## 5. Discussion

Wavelet analysis, a booming approach to studying spatial pattern, widely used in mathematics and physics for signal analysis, has started to make its way into the applied statistical and ecological literature. Despite its advantages, wavelet analysis is still not a particularly favorite technique, and only involved in several works for detection of patterns. Some gaps exist between wavelet analysis and spatial pattern analysis.

The vast majority of statistical analyses in spatial point processes assume isotropy without checking/testing for it. In practice, the goodness-of-fit of a fitted (isotropic) model is often assessed through graphical methods (see, e.g., Diggle, 2003). Unfortunately, these methods typically have little power in detecting an inadequate fit due to anisotropy. We note that anisotropy has been extensively studied in geostatistics (i.e., for numerical spatial data). It is well understood that misspecifying an isotropic model as anisotropic may result in inappropriate spatial modeling and/or less efficient spatial prediction.

Here a simple adaptation of wavelet analysis is proposed for the detection of anisotropy in point patterns. The directional scalogram within the more general context of directional wavelets seems to be very good at identifying anisotropic patterns in point location data.

Our method has been described for the analysis of univariate patterns. Multivariate point pattern analysis (e.g. analysing the relative spatial distribution of two plant species) is another strong area of interest in environmental problems. Many existing point pattern analysis methods can easily be adapted to multivariate data (Diggle, 2003), including some of those for anisotropy. The current method could also clearly be adapted to multivariate data by repeating the analysis such that only points of a specific type are used as foci and only points of a different type (for example) are counted within the sectors.

## References

Baddeley, A., Gregori, P., Mateu, J., Stoica, R. and Stoyan, D. (eds.) (2006). Case Studies in Spatial Point Process Modeling. *Lecture Notes in Statistics*, **185**, Springer-Verlag, New York.

Blackwell, P.G. (2001). Bayesian inference for a random tessellation process. *Biometrics*, **57**, 502507.

Blackwell, P.G. and Møller, J. (2002). Bayesian analysis of deformed tessellation models. *Advances in Applied Probability*, **35**, 426.

Brosofske, K.D., Chen, J., Crow, T.R. and Saunders, S.C. (1999). Vegetation responses to landscape structure at multiple scales across a Northern Wisconsin, USA, pine barrens landscape. *Plant Ecology*, **143**, 203-318.

Cliff, A.D. and Ord, J.K. (1981). *Spatial Processes. Models and Applications.* Pion, London.

De Miranda, J.C.S. (2003). Probability density functions of the empirical wavelet coefficients of a wavelet multidimensional Poisson intensity estimator. *Brazilian Journal of Probability and Statistics*, **22**, 157164.

Diggle, P.J. (2003). *Statistical Analysis of Spatial Point Patterns.* Arnold, London.

Diggle, P.J. and Richardson, S. (1993). Epidemiological studies of industrial pollutants: an introduction. *International Statistical Review*, **61**, 203-206.

Donoho, D.L. (1993). Nonlinear wavelet methods for recovery of signals, densities, and spectra from indirect and noisy data. In: Daubechies, I. (ed.), *Different Perspectives on Wavelets.* American Mathematical Society, pp. 173-205.

Gao, W. and Li, B.L. (1993). Wavelet analysis of coherent structures at the atmosphere-forest interface. *Journal of Applied Meteorology*, **32**, 1717-1725.

Gelfand, A.E., Diggle, P.J., Fuentes, M. and Guttorp, P. (eds.) (2010). *Handbook of Spatial Statistics*. Boca Raton: Chapman & Hall/CRC.

Goodall, D.W. (1952). Some considerations in the use of point quadrats for the analysis of vegetation. *Australian Journal of Scientific Research B, Biological Sciences*, **5**, 1-41.

Grenfell, N., Bjrnstad, B.T.O. and Kappey, J. (2001). Travelling waves and spatial hierarchies in measles epidemics. *Nature*, **414**, 716-723.

Guan, Y., Sherman, M., and Calvin, J.A. (2004). A nonparametric test for spatial isotropy using subsampling. *Journal of the American Statistical Association, Theory and Methods*, **99**, 810-821.

Guan, Y., Sherman, M. and Calvin, J.A. (2006). Assessing isotropy for spatial point processes. *Biometrics*, **62**, 119-125.

Haar, A. (1910). Zur Theorie der orthogonalen Funktionensysteme. *Mathematische Annalen*, **69**, 331-371.

Harper, K.A. and Macdonald, S.E. (2001). Structure and composition of riparian boreal forest: new methods for analyzing edge influence. *Ecology*, **82**, 649-659.

Hooder, I. and Orton, C. (1976). *Spatial Analysis in Archaeology*, Cambridge University Press.

Illian, J., Penttinen, A., Stoyan, H. and Stoyan, D. (2008). *Statistical Analysis and Modeling of Spatial Point Patterns*. Wiley & Sons, Chichester.

Kovalev, V.A. and Bondar, Y.S. (1997). A method for anisotropy analysis of 3D images. *Lecture Notes in Computer Science*, Vol. **1296**. Proceedings of the 7th International Conference on Computer Analysis of Images and Patterns, Springer Berlin/Heidelberg, 495-502.

Kumar, P. (1995), A wavelet based methodology for scale-space anisotropic analysis. *Geophys. Res. Lett.*, **22**, 2777-2780.

Mallat, S. (1999). *A wavelet tour of signal processing.* Elsevier, Second Edition.

Mateu, J. (2000). Second-order characteristics of spatial marked processes with applications. *Nonlinear Analysis: Real World Applications*, **1**, 145-162.

Miriti, M.N., Howe, H.F. and Wright, S.J. (1998). Spatial patterns of mortality in a Colorado desert plant community. *Plant Ecololy*, **136**, 41-51.

Møller, J. and Rasmussen, J.G. (2009). Modelling point patterns with linear structures. *Stereology and Image Analysis. Ecs10: Proceedings of The 10th European Congress of ISS.* V. Capasso *et al.* (eds)., 273-278.

Goupillaud, P., Grossman, A. and Morlet, J. (1984). Cycle-octave and related transforms in seismic signal analysis. *Geoexploration*, **23**, 85-102.

Mugglestone, M. and Renshaw, E. (1998). Detection of geological lineations on aerial photographs using two-dimensional spectral analysis. *Computers and Geosciences*, **24**, 771-784.

Neyman, J. and Scott, E.L. (1958). Statisical approach to problems of cosmology (with discussion). *Journal of the Royal Statistical Society B*, **20**, 1-43.

Neupauer, R.M. and Powell, K.L. (2005). A fully-anisotropic Morlet wavelet to identify dominant orientations in a porous medium. *Computers and Geosciences*, **31**, 465-471.

Ogata, Y. (1998). Spacetime point process models for earthquake occurrences. *Annals of the Institute of Statistical Mathematics*, **50**, 379-402.

Ohser, J. and Stoyan, D. (1981). On the second-order and orientation analysis of planar stationary point processes. *Biometrical Journal*, **23**, 523-533.

Penttinen, A. and Stoyan, D. (1989). Statistical analysis for a class of line segment processes. *Scandinavian Journal of Statistics*, **16**, 153-168.

Perry, J.N., Liebhold, A.M., Rosenberg, M.S., Dungan, J., Miriti, M., Jakomulska, A. and

Citron-Pousty, S. (2002). Illustrations and guidelines for selecting statistical methods for quantifying spatial pattern in ecological data. *Ecography*, **25**, 578-600.

Pielou, E.C. (1977). *Mathematical Ecology.* John Wiley and Sons, New York.

Redenbach, C., Särkkä, A., Freitag, J. and Schladitz, K. (2009). Anisotropy analysis of pressed point processes. *Advances in Statistical Analysis*, **93**, 237-261.

Rosenberg, M.S. (2004). Wavelet analysis for detecting anisotropy in point patterns. *Journal of Vegetation Science*, **15**, 277-284.

Ripley, B.D. (1981). *Spatial Statistics.* John Wiley and Sons, New York.

Saunders, S.C., Chen, J., Crow, T.R. and Brofoske, K.D. (1998). Hierarchical relationships between landscape structure and temperature in a managed forest landscape. *Landscape Ecology*, **13**, 381-395.

Schenk, H.J. and Mahall, B.E. (2002). Positive and negative interactions contribute to a north-south-patterned association between two desert shrub species. *Oecologia*, **132**, 402-410.

Stoyan, D. and Benes, V. (1991). Anisotropy analysis for particle systems. *Journal of Microscopy*, **164**, 159-168.

Stoyan, D. Kendall, W. and Mecke, J. (1995). *Stochastic Geometry and its Applications.* Second Edition. Wiley, Chichester.

Vidakovic, B. (1999). *Statistical Modeling by Wavelets.* Wiley & Sons, New York.

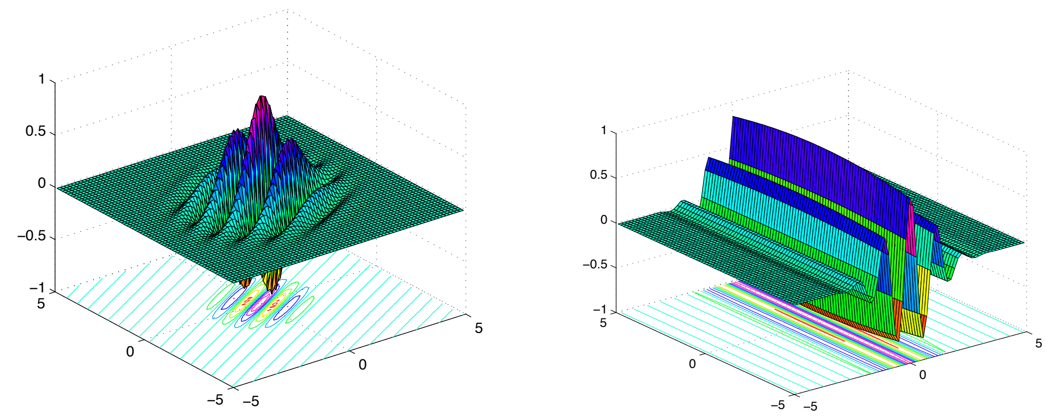

(a) (b)

**Figure 1.** Fully-anisotropic directional Morlet wavelet with parameters: (a) $D = 0.8$, $k_0 = 5.5$, $\theta = 30$, (b) $D = 0.1$, $k_0 = 5.5$, $\theta = 90$

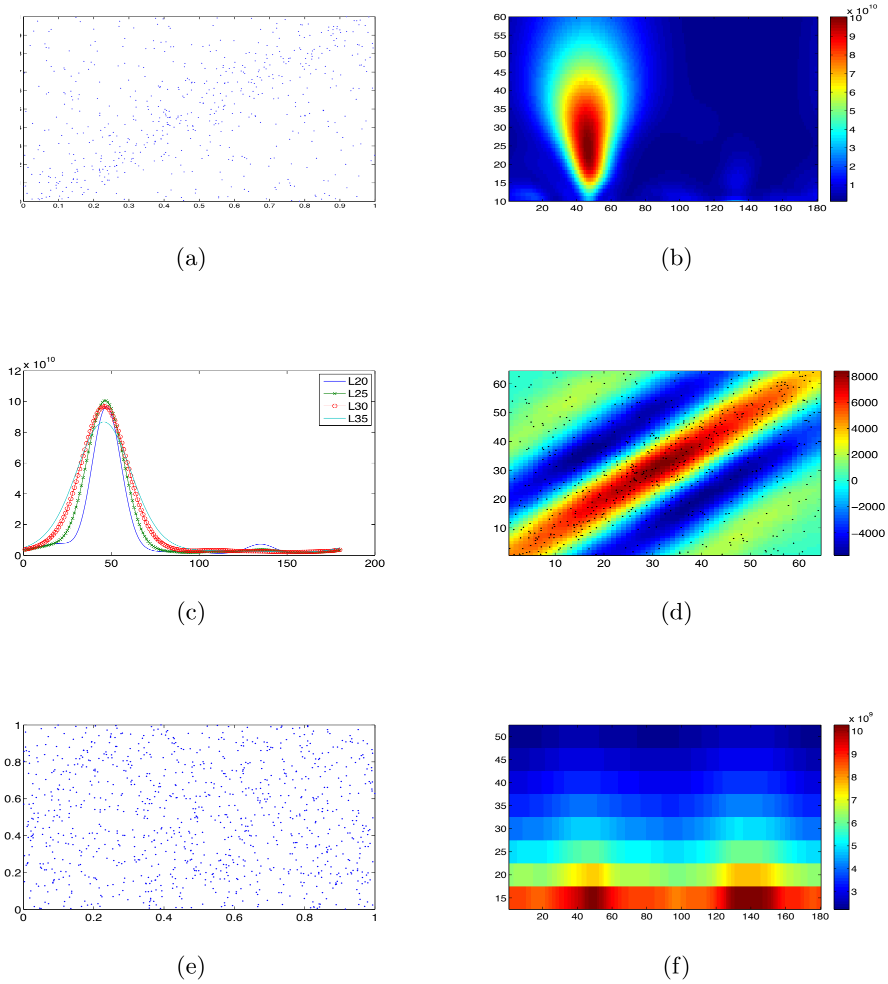


**Figure 2.** (a) Simulated spatial point pattern with $N = 1000$ points in the unit square, with a marked directional pattern of 45 degrees. (b) Values of $\eta(a, \theta)$ for the scales $a = 10, \ldots, 60$ (in ordinates) and angles $\theta = 1, \ldots, 180$ (in abscissas). (c) $\eta(a, \theta)$ function for fixed levels of resolutions (from $L = 20$ to $L = 35$). (d) Wavelet coefficients for $\theta = 45$ and scale $L = 25$. (e) Simulated isotropic random point pattern with $N = 1000$ points in the unit square. (f) Values of $\eta(a, \theta)$ for the scales $a = 15, \ldots, 50$ (in ordinates) and angles $\theta = 1, \ldots, 180$ (in abscissas)

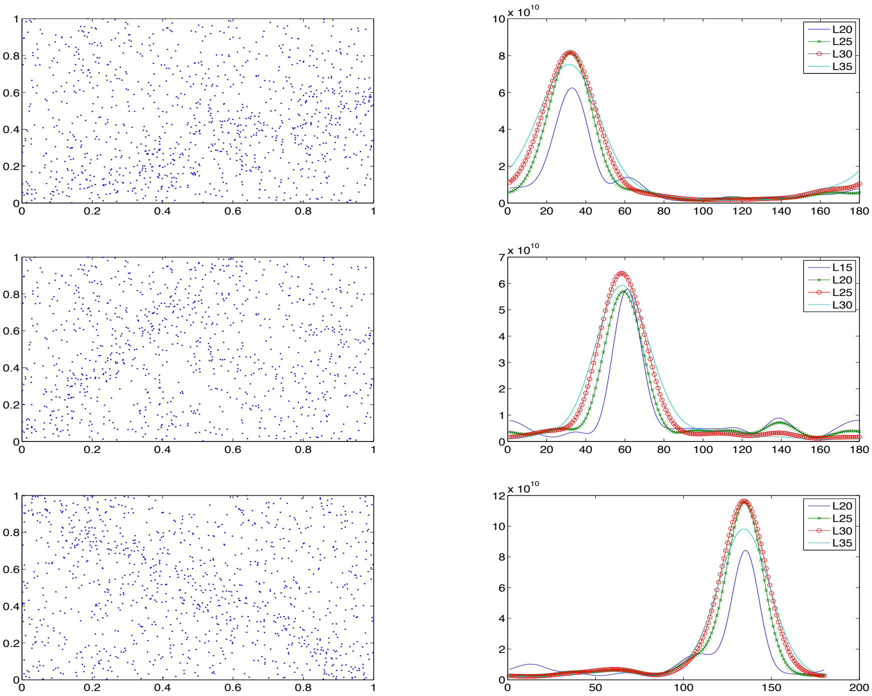


**Figure 3.** *Left column*: Simulated point patterns with $N = 1000$ points in the unit square with a marked directional pattern of 30, 60 and 135 degrees, respectively. *Right column*: $\eta(a, \theta)$ function for fixed scales and angles varying from 1 to 180 in abscissas

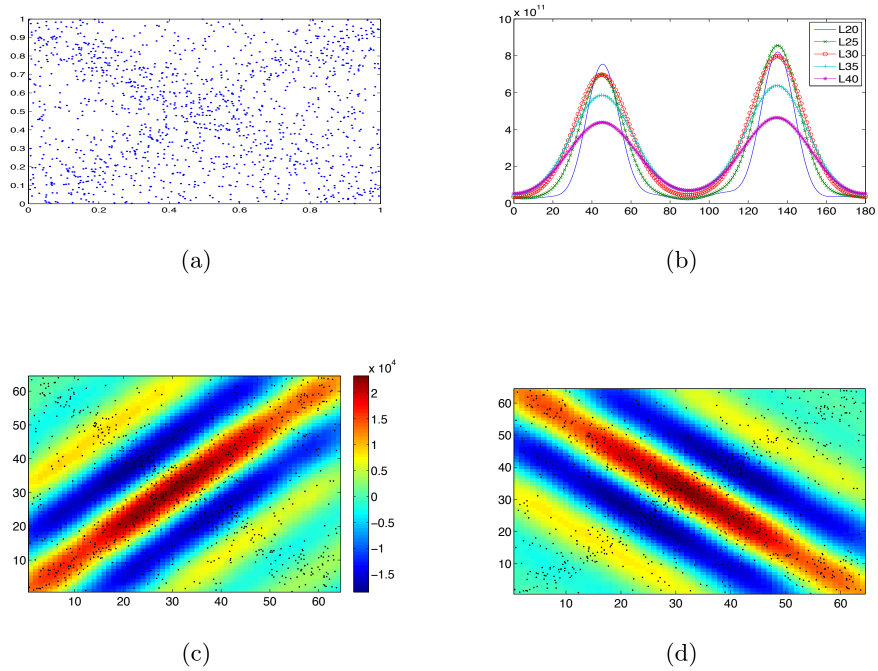


**Figure 4.** (a) Simulated spatial point pattern with $N = 1000$ points in the unit square and two perpendicular linear patterns with main directions at 45 and 135 degrees. (b) $\eta(a, \theta)$ function for several levels of resolution (from $L = 20$ to $L = 40$), and angles varying from 1 to 180. (c) Wavelet coefficients for $\theta_1 = 45$ and scale $L = 20$. (d) Wavelet coefficients for $\theta_2 = 135$ and scale $L = 25$

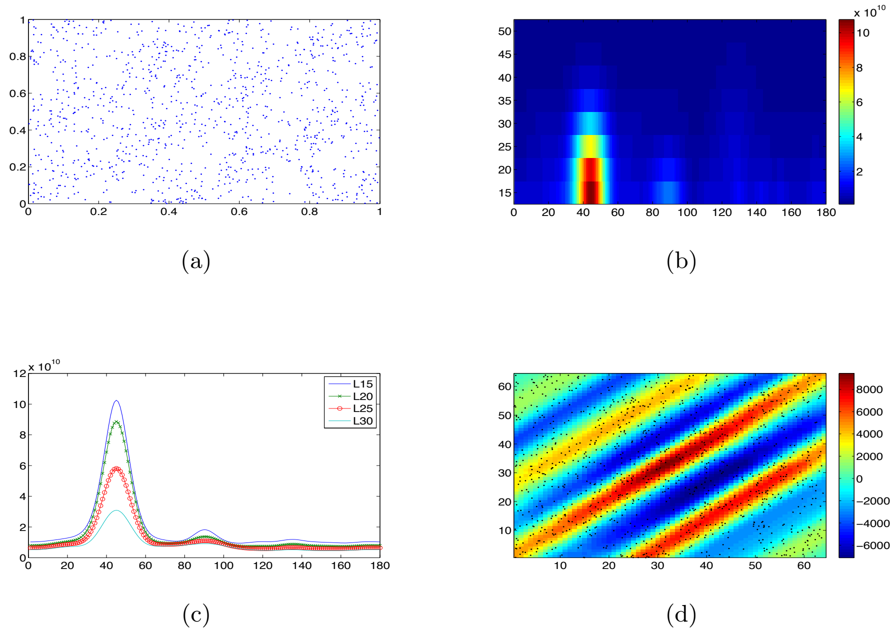


**Figure 5.** (a) Simulated striped spatial point pattern with $N = 1000$ points in the unit square with a marked directionality of 45 degrees. (b) Values of $\eta(a, \theta)$ function for scales $a = 15, \ldots, 50$ (in ordinates) and angles varying from 1 to 180 (in abscissas). (c) $\eta(a, \theta)$ function for some fixed levels of resolution ($L = 15$ to $L = 30$). (d) Wavelet coefficients for $\theta = 45$ and scale $L = 15$

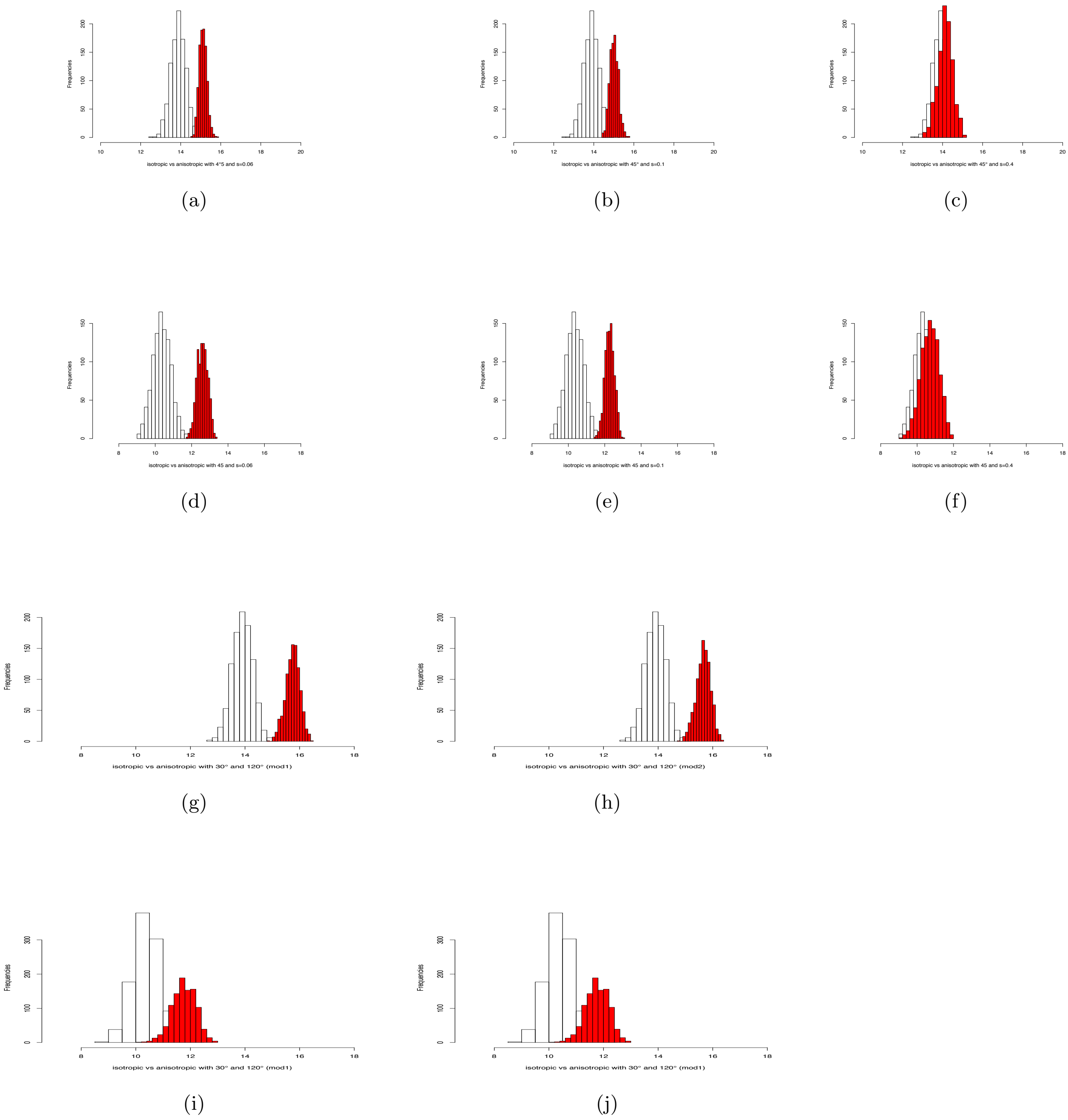


**Figure 6.** Empirical distributions of $T(\theta_i)$ for a particular $\theta_i$ under isotropy (white) and anisotropy (red) for spatial data sets with 1000 (*first and third rows*) and 300 (*second and fourth rows*) points in the unit square. The anisotropic patterns were defined through a main marked directionality at 45 degrees with $\sigma = 0.06$ (a,d), $\sigma = 0.1$ (b,e), and $\sigma = 0.4$ (c,f), and through two marked directionalities at 30 and 120 degrees with $\sigma = (0.06, 0.10)$ (g,i) and $\sigma = (0.1, 0.06)$ (h,j)

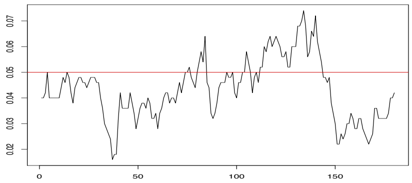

(a)

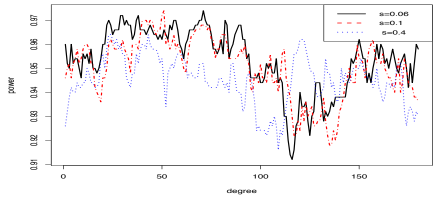


(b)

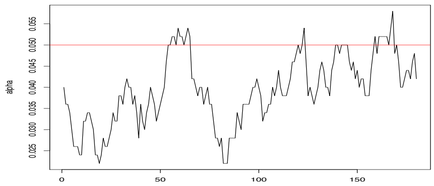


(c)

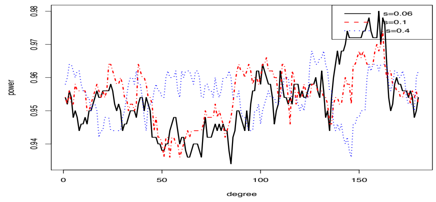


(d)

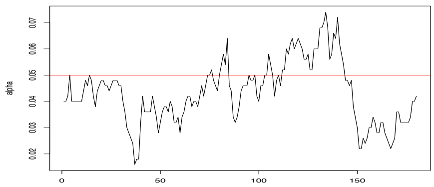


(e)

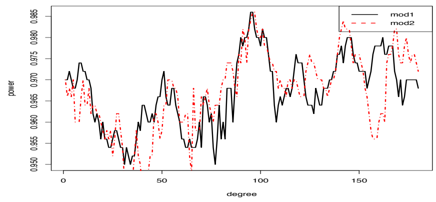


(f)

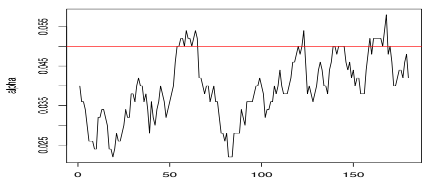


(g)

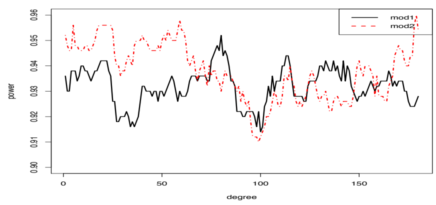


(h)

**Figure 7.** Type I error rates (*first column*) and power (*second column*) of the test for the case of $N = 1000$ (*first and third rows*) and (*second and fourth rows*) points in the unit square. Cases a-d correspond to anisotropic patterns with a main marked directionality at 45 degrees and standard deviations $\sigma = 0.06, 0.10, 0.40$. Cases e-h correspond to anisotropic patterns with two marked directionalities at 30 and 120 degrees with $\sigma = (0.06, 0.10)$ (mod1) and $\sigma = (0.1, 0.06)$ (mod2)

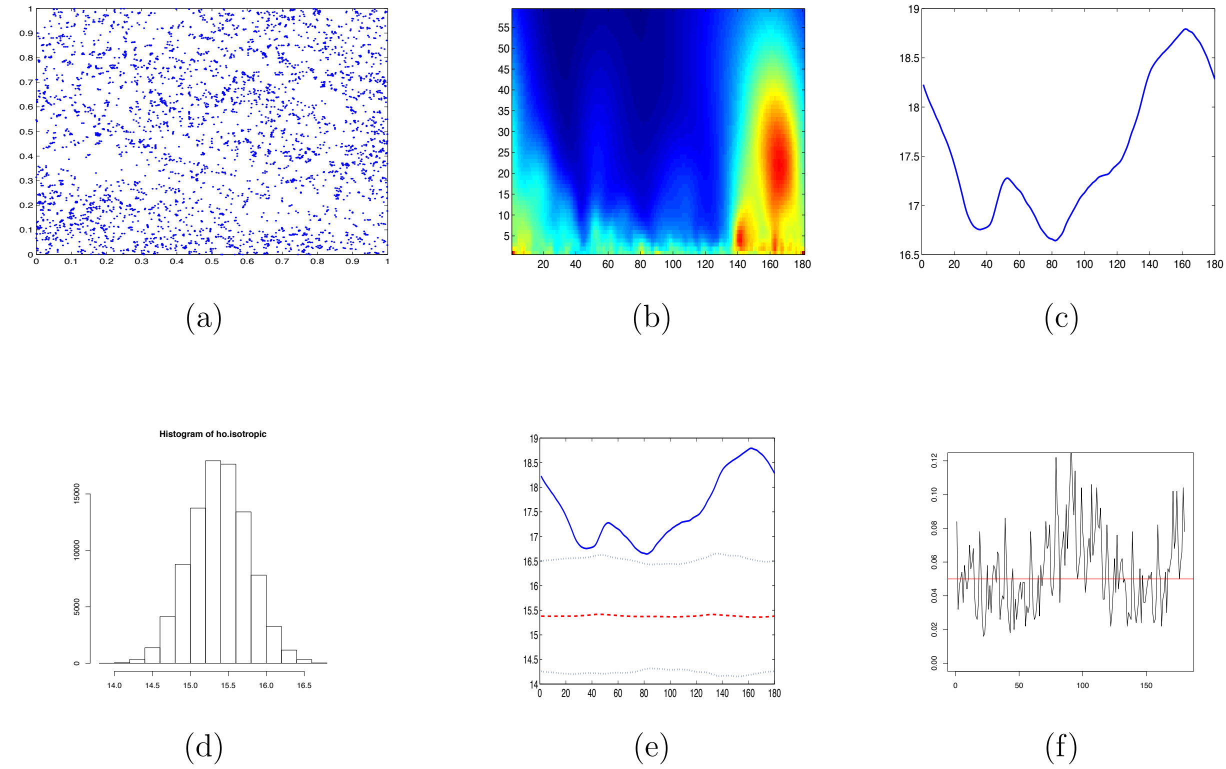


**Figure 8.** *First row*: Directional wavelet analysis for the *Ambrosia dumosa* data set in (a): (b) Directional scalogram (values of $\eta(a,\theta)$ function) for each direction and scale, and (c) Test statistic $T(\theta_i)$ for each direction $\theta_i$. *Second row*: (d) Empirical histogram of $T(\theta_i)$, $i = 1,\ldots,180$ under 1000 isotropic simulations. (e) Values of $T(\theta_i)$, $i = 1,\ldots,180$ for the *Ambrosia dumosa* data set (solid line), mean of the test statistic from 1000 simulations under isotropic Poisson processes with $\lambda = 4370$ (dashed line), and $\pm 3\sigma$ confidence intervals for the mean of the test statistic under isotropic patterns (dotted lines). (f) $p$-values for the *Ambrosia dumosa* data set compared with the dotted line at $\alpha = 0.05$

| | | Degree | | | |
|---|---|---|---|---|---|
| lev. | iso | 30 | 45 | 60 | 135 |
| 15 | 88.84 (52.73) | 30.62 (4.28) | 44.94 (2.54) | 59.66 (1.72) | 134.78 (1.49) |
| 20 | 90.89 (50.90) | 30.65 (2.07) | 44.91 (1.23) | 59.60 (1.70) | 134.93 (1.37) |
| 25 | 90.01 (50.76) | 30.54 (1.97 ) | 44.95 (1.25) | 59.32 (1.89) | 134.01 (1.41) |
| 30 | 87.90 (50.22) | 30.63 (1.87) | 44.89 (1.35) | 59.26 (1.92) | 134.89 (1.49) |
| 35 | 86.67 (51.40) | 30.33 (1.85) | 44.96 (1.61) | 59.47 (1.95) | 134.84 (1.63) |
| 40 | 86.27 (51.48) | 29.91 (1.93) | 44.96 (1.84) | 59.80 (2.07) | 134.83 (1.78) |
| 45 | 85.31 (49.82) | 29.43 (2.18) | 45.01 (1.97) | 60.12 (2.22) | 134.81 (1.90) |
| 50 | 85.31 (49.74) | 29.03 (2.37) | 45.07 (2.05) | 60.53 (2.48) | 134.81 (2.01) |

**Table 1**

*Averages and standard deviations (in parenthesis) of estimated directions from 100 repetitions of linear point patterns in the unit square with marked directions at $\theta = 30$, 45, 60 and 135 degrees.*

| | TLP1 | | TLP2 | | PP |
|---|---|---|---|---|---|
| lev. | 45 | 135 | 60 | 135 | 45 |
| 5 | 43.67 (8.04) | 134.85. (5.12) | 59.72. (0.96) | 135.32. (6.18) | 44.54 (6.67) |
| 10 | 46.22 (6.64) | 135.66 (4.47) | 59.92. (0.76) | 134.75 (3.90) | 45.00 (5.29) |
| 15 | 44.98(1.04) | 135.02 (1.00) | 59.75 (1.02) | 134.88 (1.03) | 45.05 (0.71) |
| 20 | 44.92(1.11) | 135.08 (1.08) | 59.79 (1.40) | 135.11 (1.01) | 45.01 (0.85) |
| 25 | 44.86(1.15) | 135.08 (1.16) | 59.32 (1.44) | 135.25 (1.17) | 44.99 (0.86) |
| 30 | 44.84(1.27) | 135.09 (1.23) | 59.05 (1.66) | 135.89 (1.46) | 45.98 (6.54) |
| 35 | 44.89(1.43) | 135.09 (1.34) | 59.32 (2.03) | 135.29 (1.82) | 46.1 (8.52) |
| 40 | 44.92(1.55) | 135.04 (1.45) | 59.93 (2.34) | 135.70 (2.05) | 47.68 (9.15) |
| 45 | 44.89(1.73) | 135.14 (1.57) | 60.67 (2.78) | 133.34 (2.25) | 48.71 (8.74) |
| 50 | 44.88(1.92) | 135.11 (1.79) | 61.62 (3.23) | 132.91 (2.38) | 49.03 (8.53) |

**Table 2**

*Averages and standard deviations (in parenthesis) of estimated directions from 100 repetitions of spatial patterns with* $N = 1000$ *points in the unit square with two marked directions at* $(\theta = 30, \theta = 135)$ *(TLP1), at* $(\theta = 60, \theta = 135)$ *(TLP2), and five parallel patterns at* $(\theta = 45)$ *(PP)*